Draft version December 1, 2022
Typeset using LaTeX default style in AASTeX63

TESS Asteroseismic Analysis of HD 76920: The Giant Star Hosting An Extremely Eccentric Exoplanet

Chen Jiang(姜晨) [1], Tao Wu (吴涛) [2,3,4,5,6], Adina D. Feinstein [7,*], Keivan G. Stassun [8], Timothy R. Bedding [9,10], Dimitri Veras [11,12,13], Enrico Corsaro [14], Derek L. Buzasi [15], Dennis Stello [16,9,10], Yaguang Li(李亚光) [9,10], Savita Mathur [17,18], Rafael A. García [19], Sylvain N. Breton [20], Mia S. Lundkvist [21], Przemysław J. Mikołajczyk [22,23], Charlotte Gehan [1,24], Tiago L. Campante [24,25], Diego Bossini [24], Stephen R. Kane [26], Jia Mian Joel Ong (王加冕) [27], Mutlu Yildiz [28], Cenk Kayhan [29], Zeynep Çelik Orhan [28], Sibel Örtel [28], Xinyi Zhang (张昕旖) [30], Margarida S. Cunha [24,25], Bruno Lustosa de Moura [31,32], Jie Yu (余杰) [1], Daniel Huber [33], Jian-wen, Ou (欧建文) [34], Robert A. Wittenmyer [35], Laurent Gizon [1,36,37] and William J. Chaplin [10,38]

[1] *Max-Planck-Institut für Sonnensystemforschung, Justus-von-Liebig-Weg 3, 37077 Göttingen, Germany*
[2] *Yunnan Observatories, Chinese Academy of Sciences, 396 Yangfangwang, Guandu District, Kunming, 650216, People's Republic of China*
[3] *Key Laboratory for the Structure and Evolution of Celestial Objects, Chinese Academy of Sciences, 396 Yangfangwang, Guandu District, Kunming, 650216, People's Republic of China*
[4] *Center for Astronomical Mega-Science, Chinese Academy of Sciences, 20A Datun Road, Chaoyang District, Beijing, 100012, People's Republic of China*
[5] *University of Chinese Academy of Sciences, Beijing 100049, People's Republic of China*
[6] *Institute of Theoretical Physics, Shanxi University, Taiyuan 030006, China*
[7] *Department of Astronomy and Astrophysics, University of Chicago, 5640 S. Ellis Ave, Chicago, IL 60637, USA*
[8] *Department of Physics and Astronomy, Vanderbilt University, Nashville, TN 37235, USA*
[9] *Sydney Institute for Astronomy (SIfA), School of Physics, University of Sydney, NSW 2006, Australia*
[10] *Stellar Astrophysics Centre (SAC), Department of Physics and Astronomy, Aarhus University, Ny Munkegade 120, 8000 Aarhus C, Denmark*
[11] *Centre for Exoplanets and Habitability, University of Warwick, Coventry CV4 7AL, UK*
[12] *Centre for Space Domain Awareness, University of Warwick, Coventry CV4 7AL, UK*
[13] *Department of Physics, University of Warwick, Coventry CV4 7AL, UK*
[14] *INAF — Osservatorio Astrofisico di Catania, via S. Sofia 78, 95123 Catania, Italy*
[15] *Department of Chemistry & Physics, Florida Gulf Coast University, 10501 FGCU Boulevard S., Fort Myers, FL 33965, USA*
[16] *School of Physics, University of New South Wales, NSW 2052, Australia*
[17] *Instituto de Astrofísica de Canarias (IAC), E-38205 La Laguna, Tenerife, Spain*
[18] *Universidad de La Laguna (ULL), Departamento de Astrofísica, E-38206 La Laguna, Tenerife, Spain*
[19] *Université Paris-Saclay, Université Paris Cité, CEA, CNRS, AIM, 91191, Gif-sur-Yvette, France*
[20] *Département d'Astrophysique/AIM, CEA/IRFU, CNRS/INSU, Univ. Paris-Saclay & Univ. de Paris, 91191 Gif-sur-Yvette, France*
[21] *Stellar Astrophysics Centre (SAC), Department of Physics and Astronomy, Aarhus University, Ny Munkegade 120, DK-8000 Aarhus C, Denmark*
[22] *Astronomical Observatory, University of Warsaw, Al. Ujazdowskie 4, 00-478 Warsaw, Poland*
[23] *Astronomical Institute, University of Wrocław, Mikołaja Kopernika 11, 51-622 Wrocław, Poland*
[24] *Instituto de Astrofísica e Ciências do Espaço, Universidade do Porto, Rua das Estrelas, 4150-762 Porto, Portugal*
[25] *Departamento de Física e Astronomia, Faculdade de Ciências da Universidade do Porto, Rua do Campo Alegre, s/n, 4169-007 Porto, Portugal*
[26] *Department of Earth and Planetary Sciences, University of California, Riverside, CA 92521, USA*
[27] *Department of Astronomy, Yale University, P.O. Box 208101, New Haven, CT 06520-8101, USA*
[28] *Department of Astronomy and Space Sciences, Science Faculty, Ege University, 35100, Bornova, İzmir, Türkiye*
[29] *Department of Astronomy and Space Sciences, Science Faculty, Erciyes University, 38030, Melikgazi, Kayseri, Türkiye*
[30] *State Key Laboratory of Lunar and Planetary Sciences, Macau University of Science and Technology, Macau, People's Republic of China*

Corresponding author: Chen Jiang
jiangc@mps.mpg.de

Corresponding author: Tao Wu
wutao@ynao.ac.cn

[31] Departamento de Fisica, Universidade Federal do Rio Grande do Norte, 59072-970 Natal, RN, Brazil
[32] Instituto Federal do Rio Grande do Norte—IFRN, Brazil
[33] Institute for Astronomy, University of Hawai'i, 2680 Woodlawn Drive, Honolulu, HI 96822, USA
[34] School of Physics and Electromechanical Engineering, Shaoguan University, 512005 Shaoguan, Guangdong Province, China
[35] University of Southern Queensland, Centre for Astrophysics, USQ Toowoomba, QLD 4350, Australia
[36] Institut für Astrophysik, Georg-August-Universität Göttingen, Friedrich-Hund-Platz 1, 37077 Göttingen, Germany
[37] Center for Space Science, NYUAD Institute, New York University Abu Dhabi, Abu Dhabi, UAE
[38] School of Physics and Astronomy, University of Birmingham, Birmingham B15 2TT, UK

ABSTRACT

The Transiting Exoplanet Survey Satellite (TESS) mission searches for new exoplanets. The observing strategy of TESS results in high-precision photometry of millions of stars across the sky, allowing for detailed asteroseismic studies of individual systems. In this work, we present a detailed asteroseismic analysis of the red giant star HD 76920 hosting a highly eccentric giant planet ($e = 0.878$) using 5 sectors TESS light curve that cover around 140 days of data. Solar-like oscillations in HD 76920 are detected around 52 μHz by TESS for the first time. By utilizing asteroseismic modeling that takes classical observational parameters and stellar oscillation frequencies as constraints, we determined improved measurements of the stellar mass ($M_\star = 1.22 \pm 0.11 M_\odot$), radius ($R_\star = 8.68 \pm 0.34\, R_\odot$), and age ($5.2 \pm 1.4$ Gyr). With the updated parameters of the host star, we update the semi-major axis and mass of the planet as $a = 1.165 \pm 0.035$ au and $M_\mathrm{p} \sin i = 3.57 \pm 0.22\, M_\mathrm{Jup}$. With an orbital pericenter of 0.142 ± 0.005 au, we confirm that the planet is currently far away enough from the star to experience negligible tidal decay until being engulfed in the stellar envelope. We also confirm that this event will occur within about 100 Myr, depending on the stellar model used.

Keywords: asteroseismology — stars: individual (HD 76920) — planets and satellites: dynamical evolution and stability

1. INTRODUCTION

The excellent quality of photometric data from space observation missions, such as CoRoT (Baglin et al. 2006) and Kepler (Borucki et al. 2010), allow for major advancements in the understanding of stellar interior physics and evolution using asteroseismology. Asteroseismology is the study of internal structure of stars by the interpretation of their oscillation frequencies. In particular, the detection of oscillations in solar-type and red giant stars has led to breakthroughs such as the discovery of fast core rotation (Beck et al. 2012) and a way to distinguish between hydrogen-shell-burning stars and stars that are also burning helium in their cores (Bedding et al. 2011).

The advent of space photometry has also brought in advancements of data analysis techniques (e.g., Davies & Miglio 2016; Lund et al. 2017; Corsaro & De Ridder 2014; Corsaro et al. 2015) and stellar modeling strategies (e.g., Serenelli et al. 2017; Silva Aguirre et al. 2017). Furthermore, by using individual oscillation frequencies as constraints in the model optimization process (Metcalfe et al. 2010; Jiang et al. 2011; Mathur et al. 2012; Paxton et al. 2013; Rendle et al. 2019), asteroseismic modeling has proven to be a robust tool to determine fundamental stellar properties, including stellar distances (Silva Aguirre et al. 2012; Rodrigues et al. 2014), radii and masses (Casagrande et al. 2014; Pinsonneault et al. 2014; Sharma et al. 2016), and most importantly ages for red giants and clump stars (Casagrande et al. 2016; Anders et al. 2017; Pinsonneault et al. 2018). Consequently, this enables us to characterize systematically the properties of the exoplanet-host stars through asteroseismology, which in turn provides an unprecedented level of precision in the parameters estimated for the planets (Ballard et al. 2014; Campante et al. 2015; Lundkvist et al. 2016; Kayhan et al. 2019). Furthermore, the synergy between asteroseismology and exoplanetary research also enables us to set constraints on the spin-orbit alignment of exoplanet systems (Huber et al. 2013; Benomar et al. 2014; Chaplin et al. 2014; Lund et al. 2014; Campante et al. 2016a; Kamiaka et al. 2019) and to perform statistical inferences on the planetary orbital eccentricities, by making use of asterodensity profiling (Kane et al. 2012; Sliski & Kipping 2014; Van Eylen & Albrecht 2015; Van Eylen et al. 2019).

* NSF Graduate Research Fellow

The Transiting Exoplanet Survey Satellite (TESS) Mission (Ricker et al. 2015) is NASA's near all-sky survey for exoplanets, which launched in 2018. The large sample of monitored systems guarantees the synergy between asteroseismology and exoplanetary science to continue to expand (Campante et al. 2018; Huber 2018; Hatt et al. 2022). TESS searches for exoplanets using the transit method in an area 400 times larger than that covered by the Kepler mission. Although the exploration of new exoplanetary systems is the main scientific goal of the mission, TESS has also provided aids toward the characterization of previously known systems (Kane et al. 2021). Thanks to the high-quality of TESS photometry and large sky coverage, oscillations are expected to be detected in hundreds of thousands of solar-like oscillators (Campante et al. 2018; Huber 2018; Schofield et al. 2019), including several hundred asteroseismic exoplanet hosts (Campante et al. 2016b). Detections of oscillations by TESS in previously known exoplanet-host stars were reported by several works (e.g. Campante et al. 2019; Jiang et al. 2020b; Nielsen et al. 2020; Hill et al. 2021; Huber et al. 2022), following on the discovery of the first planet transiting a star (TOI-197) in which oscillations could be measured by TESS (Huber et al. 2019).

In this work, using TESS data, we present an asteroseismic analysis of the K giant star HD 76920 (TIC 302372658) known to host a planet. At the time that HD 76920 b was first detected through the radial-velocity (RV) survey of Pan-Pacific Planet Search (Wittenmyer et al. 2017), it was the most eccentric exoplanet known to orbit an evolved star, with an orbital eccentricity of 0.856 ± 0.009. Later, with the help of new multi-site RV measurements, Bergmann et al. (2021) refined the planetary properties, finding an even higher eccentricity of 0.8783 ± 0.0025 and an orbital period of $415.891^{+0.043}_{-0.039}$ days, a minimum planet mass of $3.13^{+0.41}_{-0.43}\,M_{\rm Jup}$, and a semi-major axis of $1.091^{+0.068}_{-0.077}$ au. There is no evidence of any unseen binary companion, suggesting a scattering event rather than Kozai oscillations as the probable explanation for the observed eccentricity, and making the system valuable to the study the evolution and occurrence of planets around evolved stars. TESS detected solar-like oscillations in HD 76920 for the first time. Bergmann et al. (2021) analyzed three sectors (9, 10 and 11) of TESS data and estimated the stellar mass and radius through the scaling relations (Brown & Gilliland 1990; Kjeldsen & Bedding 1995; Stello et al. 2008; Kallinger et al. 2010) using the measurements of global seismic parameters. While the scaling relations provide decent estimates of the stellar mass and radius for stars showing solar-like oscillations, improvements, in terms of accuracy and precision, of the estimates can be achieved by using asteroseismic modeling and individual oscillation modes.

In this paper, we aim to analyze the solar-like oscillations from 5 sectors of TESS photometric light curve. Including these oscillations in detailed stellar modeling can help us derive precise fundamental stellar properties of the host star. The improved stellar parameters can further be used to update the properties of the orbiting planet, which is of great importance in characterizing the planetary system. The determined stellar age from asteroseismology and modeling can provide information about the evolution of the system, which assists at predicting the final fate of the planet.

2. OBSERVATIONS

2.1. *TESS Observations*

HD 76920 has been observed by TESS in Sectors 9, 10, 11 at 30-min cadence during its Cycle 1 observations, and Sectors 36 and 37 at 10-min cadence[1] during its Cycle 3 observations. To extract these light curves, we used the open-source Python package `eleanor` (v2.0.3; Feinstein et al. 2019)[2]. `eleanor` performs background subtraction, systematics corrections, and aperture selection per each sector of data. We extracted 13×13 pixels postage stamps and applied the `eleanor` default apertures for light curve extraction (top panel of Figure 1). Although the aperture selection process is optimized for exoplanet searches, we found also these default apertures to perform well for asteroseismic measurements.

We used the `eleanor` corrected flux; this flux option corrects for systematic issues by regressing against a linear model of time, background, and position and removing trends by the co-trending basis vectors provided by the Science Process Operations Center pipeline (Jenkins et al. 2016). We additionally applied quality masks, provided by `eleanor`, to remove any bad cadences and removed outliers $\geq 7\sigma$ from the median of each light curve. The resulting light curves are shown in the bottom panel of Figure 1. No transit of the planet was detected in existing TESS data due to the short observation coverage compared to its long orbital period. TESS is expected to observe HD 76920 again for 5 months in Cycle 5.

[1] HD 76920 has also been observed in Sector 38 at 10-min cadence, but the data was not released at the time of this analysis.

[2] For sectors 36 and 37, `eleanor` uses the `TessCut` tool (Brasseur et al. 2019).

Table 1. Stellar Parameters for HD 76920

Parameter	Value	References
Basic Properties		
TIC	302372658	1
Hipparcos ID	43803	2
TESS Mag.	6.87	1
Sp. Type	K1 III	3
Spectroscopy		
$T_{\rm eff}$ (K)	4698 ± 100	4
	4664 ± 53	5
[Fe/H] (dex)	-0.11 ± 0.10	4
	-0.19 ± 0.06	5
$\log g$ (cgs)	2.94 ± 0.15	4
	2.71 ± 0.04	5
SED & Gaia DR3 Parallax[a]		
π (mas)	5.4618 ± 0.0187	6
A_V	0.20 ± 0.05	7
	0.15 ± 0.07	7
$F_{\rm bol}$ (erg s^{-1} cm^{-2})	$(3.12 \pm 0.11) \times 10^{-8}$	7
	$(3.08 \pm 0.11) \times 10^{-8}$	7
$R_\star$ ($R_\odot$)	8.64 ± 0.37	7
	8.70 ± 0.25	7
$L_\star$ ($L_\odot$)	32.54 ± 1.17	7
	32.06 ± 1.16	7
$M_\star$ ($M_\odot$)	1.68 ± 0.10[b]	7
Asteroseismology		
$\Delta\nu$ (μHz)	5.52 ± 0.02	7
$\nu_{\rm max}$ (μHz)	52.4 ± 0.3	7
$M_{\star,\rm seis}$ ($M_\odot$)	1.22 ± 0.11	7
$R_{\star,\rm seis}$ ($R_\odot$)	8.68 ± 0.34	7
ρ (gcc)	0.0026 ± 0.0004	7
$\log g$ (cgs)	2.648 ± 0.037	7
t (Gyr)	5.2 ± 1.4	7

[a] Two SED pipelines are used to obtain A_V, $F_{\rm bol}$, $R_\star$ and $L_\star$ (Section 2.2). The second value of each parameter is from the SEDEX pipeline (Yu et al. 2021, 2022).

[b] Based on extrapolated relations of Torres et al. (2010).

References—(1) Stassun et al. (2018b), (2) van Leeuwen (2007), (3) Houk & Cowley (1975), (4) Wittenmyer et al. (2017), (5) Bergmann et al. (2021), (6) Gaia Collaboration et al. (2021), (7) this work.

2.2. *Broadband Photometry and Spectral Energy Distribution*

As an independent determination of the basic stellar parameters, we performed an analysis of the broadband spectral energy distribution (SED) of the star together with the Gaia DR3 parallax (with no systematic offset applied; see, e.g., Stassun & Torres 2021), in order to determine an empirical measurement of the stellar radius, following the procedures

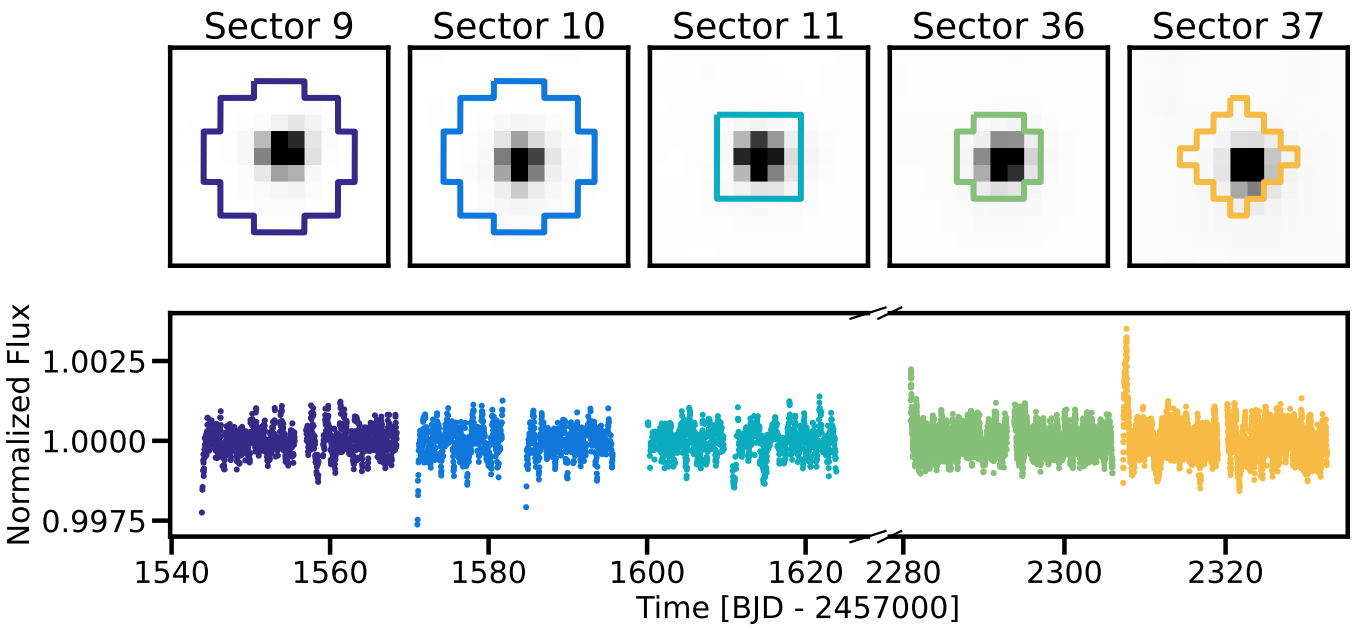

Figure 1. `eleanor` best-fit apertures (top) overlaid on the TESS target pixel files (TPFs) extracted per each sector. The TPFs are all scaled from 0 to 30000 e^{-1} s^{-1}. We use these apertures to extract the flux within `eleanor`, which are then corrected via the default `eleanor` corrected flux routine (bottom). Apertures and light curves are colored by TESS sector.

described in Stassun & Torres (2016) and Stassun et al. (2017, 2018). We pulled the $B_T V_T$ magnitudes from Tycho-2, the JHK_S magnitudes from the Two Micron All Sky Survey, the W1–W4 magnitudes from the Wide-field Infrared Survey Explorer, and the $G_{\rm BP}G_{\rm RP}$ magnitudes from Gaia DR3. Together, the available photometry spans the full stellar SED over the wavelength range 0.4–22 μm (see Figure 2).

We performed a fit using Kurucz stellar atmosphere models, with the effective temperature ($T_{\rm eff}$), surface gravity ($\log g$), and metallicity ([Fe/H]) adopted from the spectroscopic analysis of Wittenmyer et al. (2017). The remaining free parameter is the extinction A_V, which we limited to the maximum line-of-sight extinction from the Galactic dust maps of Schlegel et al. (1998). The resulting fit (Figure 2) has a reduced χ^2 of 2.2, and best-fit $A_V = 0.20 \pm 0.05$. Integrating the (unreddened) model SED gives the bolometric flux at Earth, $F_{\rm bol} = 3.12 \pm 0.11 \times 10^{-8}$ erg s^{-1} cm^{-2}. Taking the $F_{\rm bol}$ and $T_{\rm eff}$ together with the Gaia parallax, gives the stellar radius, $R_\star = 8.64 \pm 0.37\,R_\odot$, revealing the star to be clearly evolved. In addition, we can estimate the stellar mass directly from $R_\star$ together with the spectroscopic $\log g$ from (Wittenmyer et al. 2017, see Table 1), which gives $M_\star = 2.37 \pm 0.41$ M$_\odot$; this is higher than the value obtained from the empirical relations of Torres et al. (2010), giving $M_\star = 1.68 \pm 0.10$ M$_\odot$, indicating an overestimate of spectroscopic $\log g$ (see Section 4). Combining $F_{\rm bol}$ and Gaia DR3 parallax allows us to derive a luminosity $L_\star = 32.54 \pm 1.17\,L_\odot$. We also performed an independent SED fitting using the SEDEX pipeline (Yu et al. 2021, 2022) with MARCS atmosphere models (Gustafsson et al. 2008) and same input atmospheric parameters. The resulting parameters from both SED fittings are well consistent, as listed in Table 1.

3. ASTEROSEISMIC ANALYSIS

3.1. *Global Oscillation Parameters*

For the seismic analysis, the TESS light curve prepared by `eleanor` was distributed to several groups using different pipelines (e.g., Huber et al. 2009; Mathur et al. 2010; Jiang et al. 2011; Lundkvist 2015; Campante et al. 2017; Yu et al. 2018; Corsaro et al. 2020; De Moura et al. 2020; Li et al. 2020) to extract the seismic parameters. Figure 3 shows the power density spectrum of HD 76920 computed based on the `eleanor` light curve, combining both Cycle 1 and Cycle 3 data. The 10-min cadence sectors were rebinned to 30-min cadence, with a simple average over three measurements. The power spectrum shows a frequency-dependent background signal due to stellar activity, granulation, and faculae that can be modeled by a superposition of several Lorentzian-like functions (i.e., Harvey-like models, Harvey 1985; Karoff 2008; Jiang et al. 2011; Kallinger et al. 2014; Corsaro et al. 2017), and a white noise term. The background

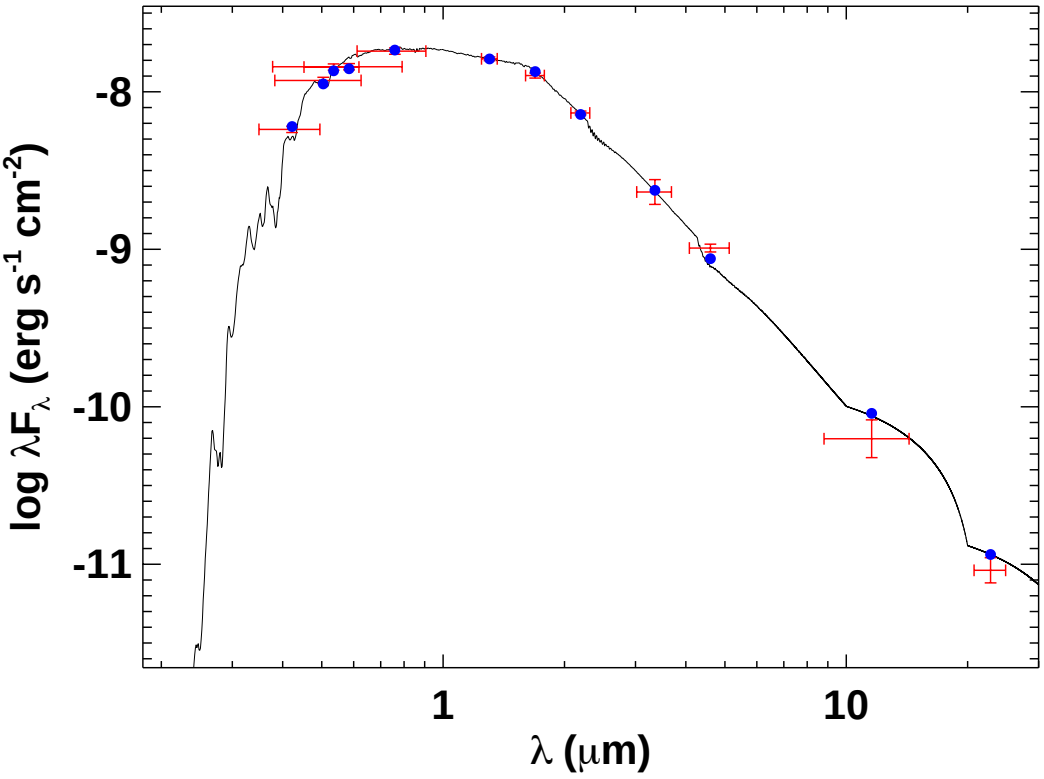

Figure 2. Spectral energy distribution of HD 76920. Red symbols represent the observed photometric measurements, where the horizontal bars represent the effective width of the passband. Blue symbols are the model fluxes from the best-fitting Kurucz atmosphere model (black).

shown as the green dotted curve in Figure 3 was obtained by fitting the background model with two Harvey-like components to the smoothed power spectrum. Since the target pixel time series of the Cycle 3 sectors have been detrended with a moving median to remove long timescale stellar variations. As a result, the background noise at low frequency is greatly suppressed during this process. Therefore, the background fit displayed in Figure 3 disregarded frequencies below $\sim$10 μHz. The global seismic parameters such as the frequency of maximum power ($\nu_{\rm max}$) and the mean large frequency separation ($\Delta\nu$) were based on the analysis of the background-corrected power spectrum generated by each group.

In general, $\nu_{\rm max}$ was measured by fitting a Gaussian distribution profile to the power excess hump of the smoothed power spectrum (e.g., Hekker et al. 2010) or through the 2D autocorrelation function (e.g., Viani et al. 2019). To measure $\Delta\nu$ techniques like autocorrelation of the amplitude spectrum (e.g., Huber et al. 2009; Mosser & Appourchaux 2009), power spectrum of the power spectrum (e.g., Kjeldsen & Bedding 1995; Mathur et al. 2010; Jiang 2015), matched filter response function (e.g., Gilliland et al. 2011), and asymptotic or linear fit to the frequencies of the radial modes (individual mode extraction given in Section 3.2) were used. However, a clear shift of the oscillation power excess region to lower frequencies is observed in the power spectrum generated with Cycle 3 data (Sectors 36 and 37), compared with the Cycle 1 one (Sectors 9 to 11), as illustrated in the upper panel of Figure 4. This is principally due to the stochastic nature of the oscillations so that the change in mode amplitudes impacts the value of $\nu_{\rm max}$. Consequently,

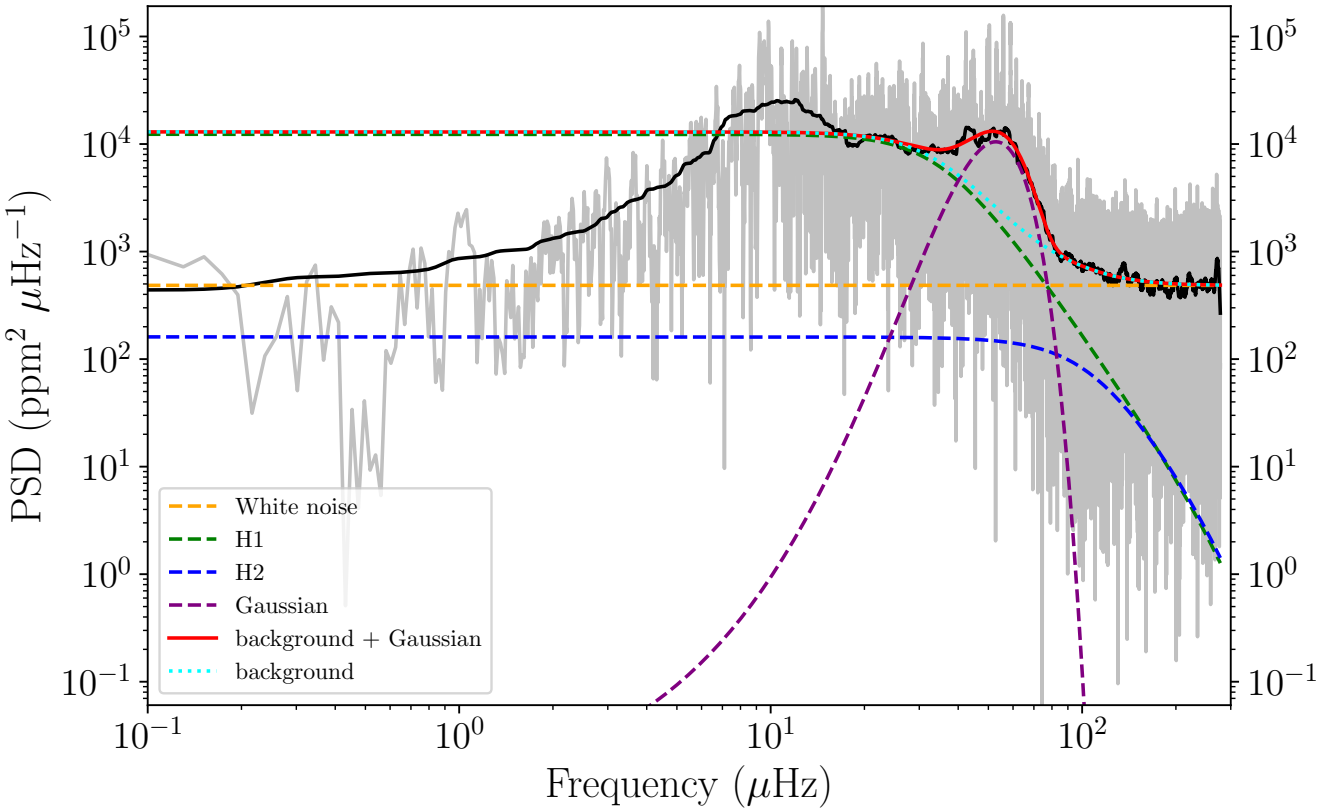

Figure 3. Power spectral density (PSD) of HD 76920 and corresponding global background model fit (green dotted curve). The background model consist of two Harvey-like profiles (cyan and blue dashed curves) and white noise (orange dashed line). The solid red curve depicts the summation of the background and a Gaussian fit (purple dashed) to the oscillation power excess envelope. The PSD is generated using 5 sectors of TESS data (Figure 1). The 10-min cadence sectors are rebinned to 30-min cadence, with simple average over three measurements. The original PSD is shown in gray and a heavily smoothed (Gaussian with an FWHM of $\Delta\nu$) version in black. The fit displayed here disregarded frequencies below $\sim$10 μHz (Section 3.1).

this shift of the power excess region would lead to large uncertainty of $\nu_{\rm max}$ when considering the corresponding formal uncertainty originate from different pipelines. Therefore, the final adopted results of the pipelines, $\nu_{\rm max} = 52.4\pm0.3\,\mu$Hz and $\Delta\nu = 5.52 \pm 0.02\,\mu$Hz, are of the smallest deviation from the mean values of all pipeline results, considering both parameters simultaneously (i.e., both parameters returned by the same pipeline). The combined power spectrum corrected from the background model is shown in the bottom panel of Figure 4, where signals with $\nu < 50\,\mu$Hz are largely enhanced by the Cycle 3 data, and those with $\nu > 50\,\mu$Hz are due to the Cycle 1 data. The asteroseismic analysis were performed based on the combined power spectrum (lower panel of Figure 4).

3.2. *Individual Mode Frequencies*

In the bottom panel of Figure 4 the combined power spectrum shows a regular series of peaks corresponding to solar-like oscillations within the frequency range between 30 to 80 μHz. To extract individual oscillation modes from the power spectrum several independent methods ranging from traditional iterative fitting of sine waves, i.e., pre-whitening (e.g. Kjeldsen et al. 2005; Lenz & Breger 2005; Bedding et al. 2007; Jiang et al. 2011), to fitting of Lorentzian mode profiles individually or in a global power spectrum model (e.g. Handberg & Campante 2011; Appourchaux et al. 2012; Mosser et al. 2012; Corsaro et al. 2015; Vrard et al. 2015; Davies & Miglio 2016; Handberg et al. 2017; Roxburgh 2017; Kallinger et al. 2018; Corsaro et al. 2020; Li et al. 2020; Breton et al. 2022) were used by different pipelines. The extracted mode frequencies and corresponding uncertainties are listed in Table 2. The extracted radial modes also allowed us to measure $\Delta\nu$ by fitting a straight line to the radial-mode frequencies. Thus, the slope of the line is $\Delta\nu$ that is $5.62 \pm 0.03\,\mu$Hz using this method. The échelle diagram generated using this $\Delta\nu$ is depicted in Figure 5. Two vertical ridges located at right edge of the figure correspond to $\ell = 0$ (red circles) and 2 (blue triangles) modes.

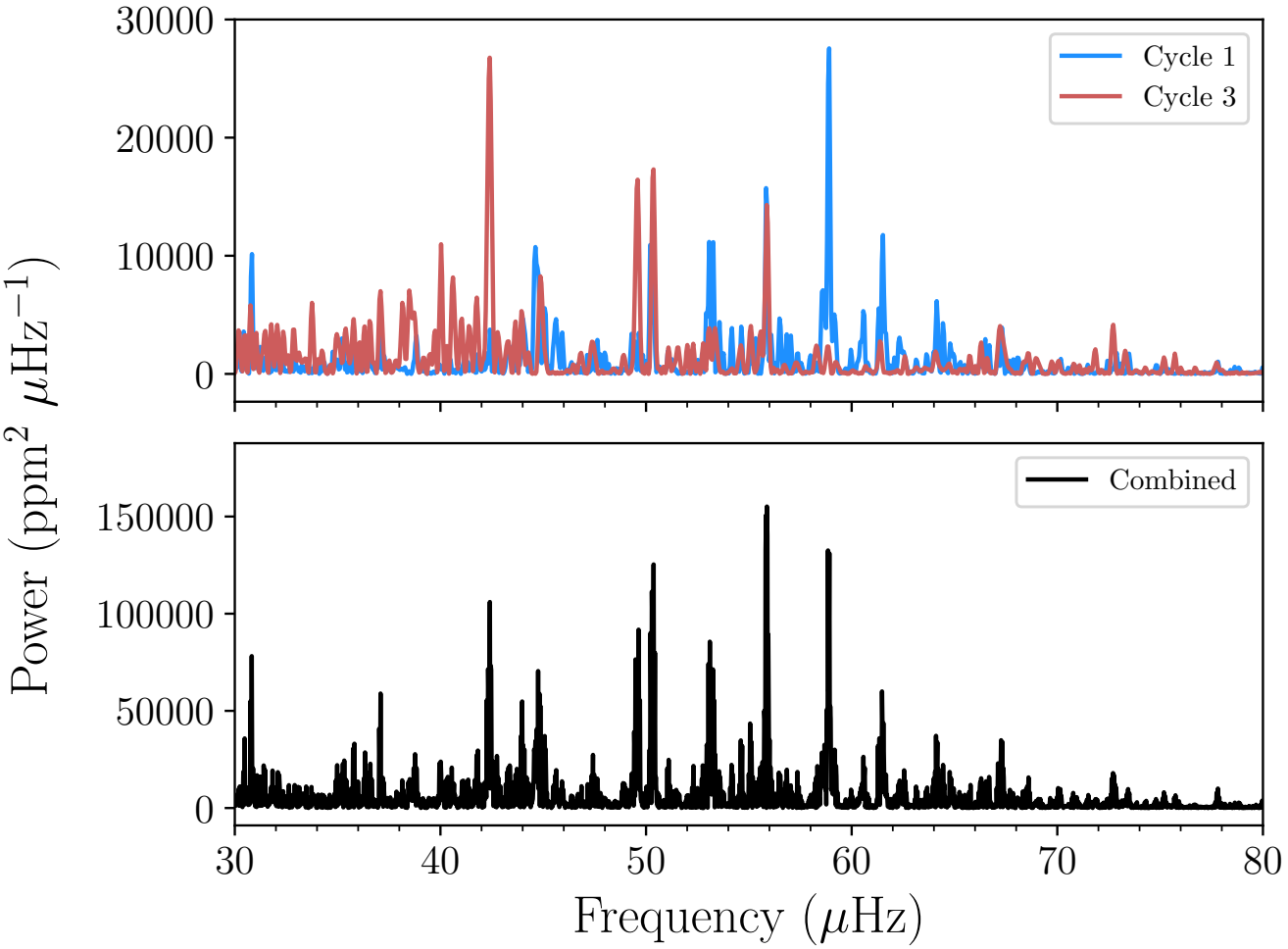

Figure 4. Background corrected power spectra of HD 76920 depicted in the power excess region. Top panel: power spectra of the Cycle 1 (Sectors 9 to 11) and Cycle 3 (Sectors 36 and 37) light curve. The Cycle 1 data shows a larger value of $\nu_{\rm max}$, compared with the Cycle 3 data. Bottom panel: power spectra of the combined light curve that is used for the asteroseismic analysis.

However, due to the relatively short duration of our TESS data for HD 76920, clear mixed-mode pattern is not visible in the power spectrum or in the échelle diagram, though there are a few peaks corresponding to $\ell = 1$ mixed modes (green diamonds) appearing in the spectrum. In Table Table 2 we also list the most significant $\ell = 1$ modes that are identified by at least two independent sources.

4. ASTEROSEISMIC MODELLING

Asteroseismic modelling is a powerful tool to estimate fundamental stellar properties. Five independent teams performed modeling efforts to search for the stellar models that best match the classical and asteroseismic constraints from observations for HD 76920. These teams employ different stellar evolution codes (ASTEC, MESA; Christensen-Dalsgaard 2008a; Paxton et al. 2011, 2013, 2015), oscillation codes (ADIPLS, GYRE Christensen-Dalsgaard 2008b; Townsend & Teitler 2013), and optimization methods (Mier 2017; Kayhan et al. 2019; Wu & Li 2019; Yıldız et al. 2019; Jiang & Gizon 2021; Zhang et al. 2022). The input physics adopted by each team is detailed in Table 3. Diffusion and overshoot were turned off except for one team. For the modeling, all five teams used the luminosity $L_\star$ of $32.54\pm1.17\,L_\odot$ derived with Gaia DR3 parallax (Section 2.2) and the spectroscopic measurements i.e., the effective temperature $T_{\rm eff}$ and metallicity [Fe/H] listed in Table 1, as constraints. As for the seismic constraints, the large frequency separation $\Delta\nu$

Table 2. Extracted Oscillation Frequencies from TESS light curve and Mode Identification based on the best-fitting model for HD 76920

ℓ	n	ν (μHz)	σ_ν (μHz)	SNR
0	7	44.80	0.13	6.63
0	8	50.32	0.10	8.08
0	9	55.85	0.08	12.50
0	10	61.48	0.08	6.71
0	11	67.18	0.13	3.83
0	12	72.73	0.15	4.0
1	6	42.41	0.08	12.05
1	8	53.12	0.03	9.54
1	8	53.27	0.03	6.73
1	9	58.90	0.07	6.95
1	10	64.13	0.08	3.61
2	5	38.61	0.29	3.71
2	6	43.93	0.24	5.88
2	7	49.53	0.12	7.13
2	8	55.10	0.07	5.42
2	9	60.59	0.20	4.48
2	10	66.32	0.07	3.89

NOTE—Each mode is labeled according to its mode degree ℓ, radial order n (radial order of acoustic-component for non-radial modes) from the best-fitting model. ν and σ_ν are the mode cyclic frequency and uncertainty. Modes presented here are all with a height-to-background ratio larger than 3 and identified by at least two independent methods/sources.

Table 3. Modeling configurations from different sources. One entry is used where all five teams used the same input physics.

team	Ong	Kayhan	Izmir	Zhang	BESTP
Evolution code	`MESA` (r12778)	`MESA` (r12778)	`MESA` (r15140)	`MESA` (r10398)	`ASTEC`
Oscillation code	`GYRE`	`ADIPLS`	`ADIPLS`	`ADIPLS`	`ADIPLS`
EoS[a]	`MESA`/OPAL	`MESA`/OPAL	`MESA`/OPAL	`MESA`/OPAL	OPAL
Surface Correction[b]	BG-2term	KB	KB	None	BG-2term
Nuclear reactions	NACRE (Angulo et al. 1999)				
High-T opacities	OPAL (Iglesias & Rogers 1993, 1996)				
Low-T opacities	Ferguson et al. (2005)				
Solar mixture[c]	GS98	AGSS09	AGSS09	GS98	AGSS09
Atmosphere[d]	Eddington gray	simple photosphere	simple photosphere	Eddington gray	Kurucz
$\alpha_{\rm MLT}$	1.83	2.175	1.828	2.0	1.7 – 2.1
Overshoot	0.006	None	None	None	None
Diffusion	Thoul et al. (1994)	None	None	None	None

[a] The `MESA`/OPAL tables are based on the 2005 update of the OPAL EoS tables (Rogers & Nayfonov 2002).

[b] The adopted methods for surface correction are Kjeldsen et al. (2008) (KB) and Ball & Gizon (2014) two-term correction (BG-2term)

[c] Solar composition given in Grevesse & Sauval (1998) (GS98) and Asplund et al. (2009) (AGSS09) are used for initial chemical composition.

[d] The atmosphere choices used in `MESA` are introduced in Paxton et al. (2011), and `ASTEC` uses the Kurucz model (Kurucz 1991) for atmosphere.

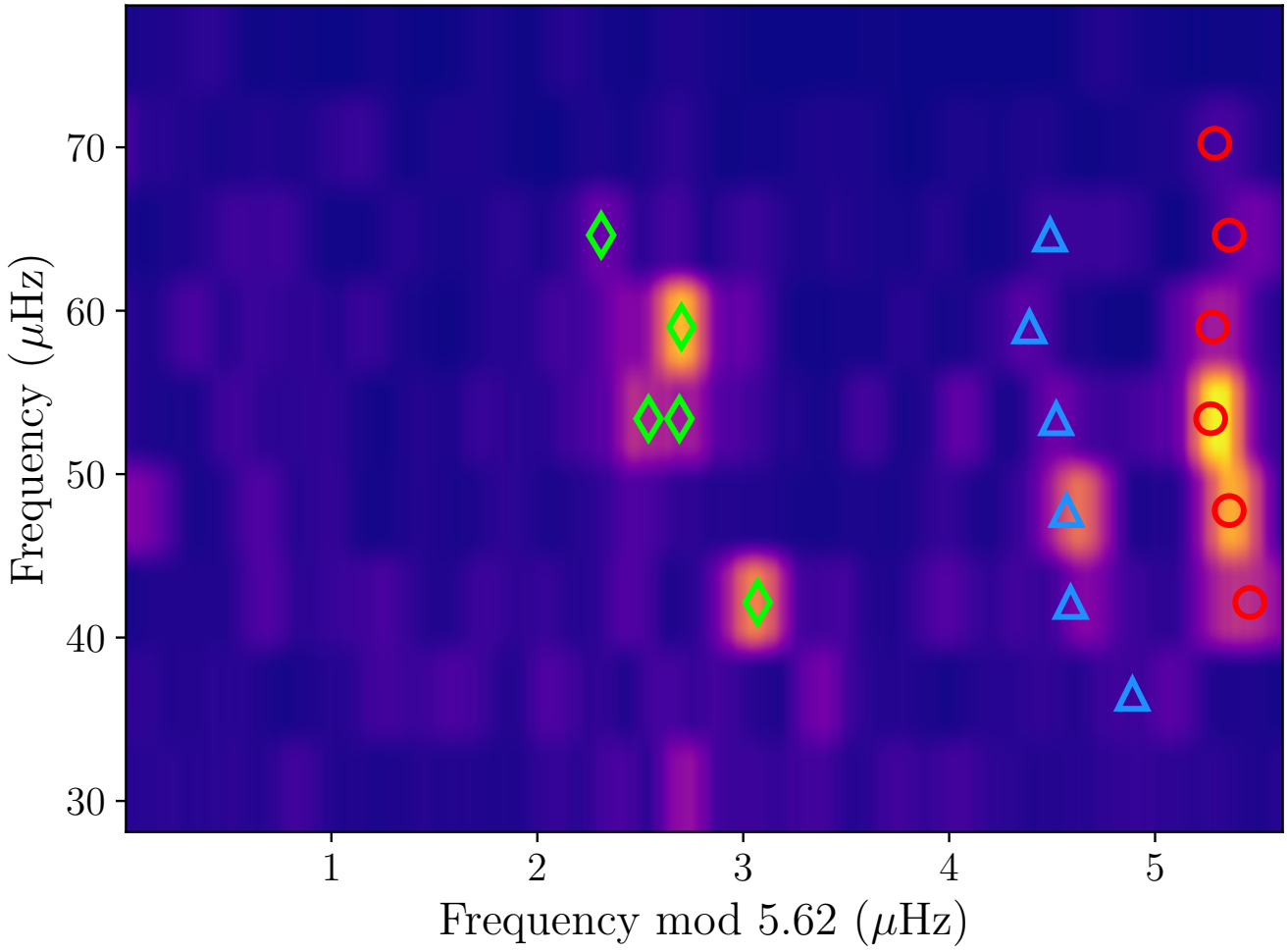

Figure 5. Grayscale échelle diagram of the background-corrected PSD. Identified individual mode (Table 2) frequencies are marked with red circles ($\ell = 0$), green diamonds ($\ell = 1$) and blue triangles ($\ell = 2$)

and $\ell = 0$ and 2 mode frequencies in Table 2 were used[3]. The constraint on $\nu_{\rm max}$ were not considered in the modeling due to the discrepancy of the oscillation power excess region between the sectors (Section 3.1). Since horizontal branch tracks (i.e. red clump stars, helium core burning) hardly crosses the observational constraints in the HR diagram, we limited the modeling to red giant branch (RGB).

The outputs from the five teams are generally in agreement with each other. The consolidated values (the mean from all sources) for stellar mass $M_{\star,\rm seis}$, radius $R_{\star,\rm seis}$, age t, surface gravity $\log g$ and density ρ are summarized in Table 1, constraining the corresponding parameters to a precision level of 9%, 4%, 27%, 1%, 15%, respectively, which are the most precise results for HD 76920 so far. The final uncertainties on these stellar parameters were recalculated by adding in quadrature the corresponding formal uncertainty for a given parameter to the standard deviation of the parameter estimates returned by all teams. Therefore, both random and systematic errors arising from the diversity of modeling codes, procedures and input physics adopted by different teams were taken into account. The estimated $\log g$ from modeling is distinctly smaller than the spectroscopic results reported by Wittenmyer et al. (2017), but matches the one measured by Bergmann et al. (2021) (who used updated spectroscopy data) within 1σ.

Figure 6 shows the locations of the sampling points by `BESTP` in the HR diagram, along with a series of evolutionary tracks with different initial masses generated by `ASTEC`. The sampling points are color-coded according to the normalized

[3] The identified five $\ell = 1$ modes listed in Table 2 do not show clear pattern of mixed modes, thus, provide very limited constraints on the models, as one can always find a match to the observed mode among the dense theoretical dipolar modes.

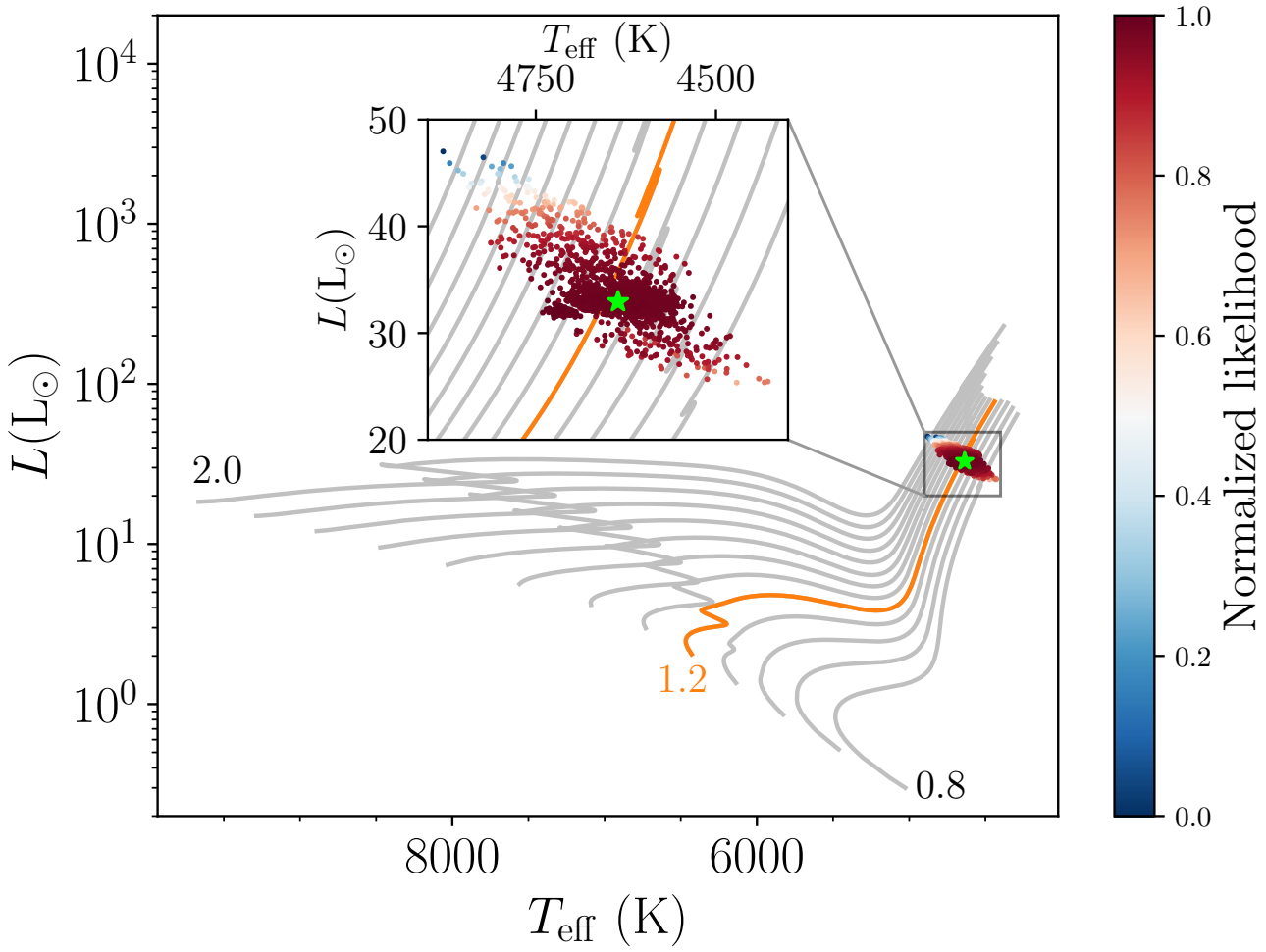

Figure 6. Evolutionary tracks for a series of `ASTEC` models with different initial masses but same chemical abundance ($X = 0.714$ and $Z = 0.0142$, corresponding to [Fe/H] = -0.09) and mixing length parameter ($\alpha = 1.927$) that are the optimization outputs of the `BESTP` pipeline. The initial masses of the models increase from 0.8 to 2.0 $M_\odot$ with a step of 0.1 $M_\odot$. The evolutionary track indicated by orange is with an initial mass of 1.2 $M_\odot$ that is closest to the adopted value (Table 1). Sampling points by `BESTP` are drawn in the diagram and also in the inset, with color-coded normalized likelihood values. The green star marks the location of our best-fitting model ($M = 1.21 M_\odot$, $X = 0.713$ and $Z = 0.0145$) from `BESTP`.

likelihood, thus, redder samples have higher possibilities as the representation of the real star. According to the figure, HD 76920 is most likely approaching closely to the RGB luminosity bump, where the properties of mixed-modes are significantly impacted by the buoyancy glitch (Cunha et al. 2015, 2019; Jiang et al. 2020a), a signature that can help us inspect the stellar mid-layer structures (Pinçon et al. 2020; Jiang et al. 2022). However, the short observation duration for HD 76920 limits the detection of mixed-modes from the TESS power spectrum, thus, such investigation of stellar interior structure with the help of mixed modes is not feasible with current TESS data. Nevertheless, by matching the theoretical oscillation frequencies calculated for the best-fitting model with the observed TESS power spectrum (Figure 7), we could confirm the mode degree and identify the mode order for $\ell = 0$ and 2 modes that were extracted by different groups (Table 2). The theoretical modes used to identify observed modes are corrected for the surface effect (e.g., Houdek et al. 2017) that yields a systematic offset between the calculated and the observed oscillation frequencies. For theoretical dipolar mixed modes, correction for the surface effect was not performed due to the lack of observed frequencies, thus, we did not show them in Figure 7.

5. CHARACTERIZATION OF HD 76920 b

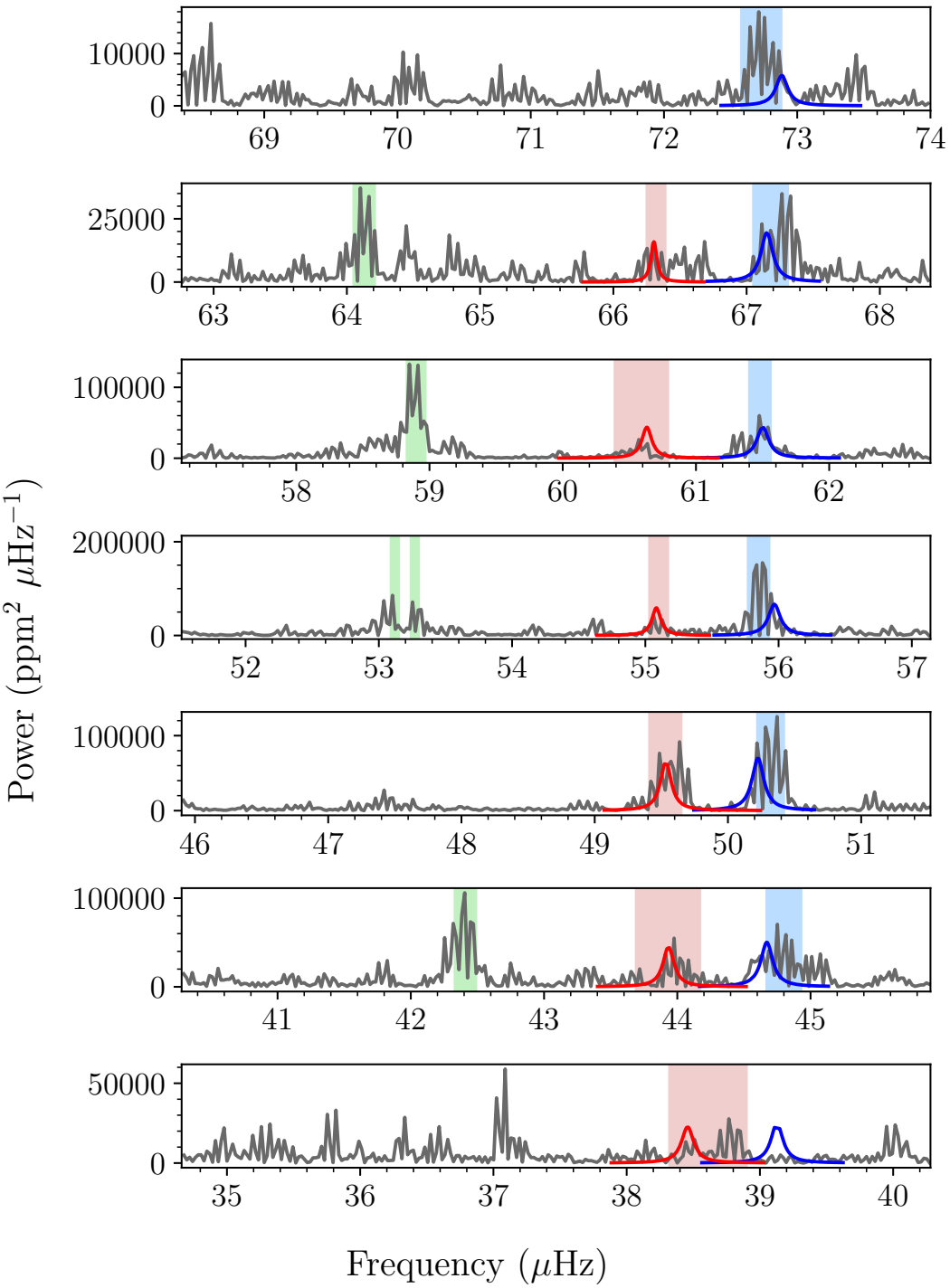

Figure 7. Background-corrected PSD (dark grey) plotted in the échelle diagram format that divides the spectrum into bins each $\Delta\nu$ wide. The blue and red peaks are the $\ell = 0$ and 2 modes, respectively, of the best-fitting model returned by `BESTP` (Figure 6). The line width and amplitude of the theoretical modes are derived using the formulae introduced in Lund et al. (2017) and Ball et al. (2018). The corresponding observed frequencies and uncertainties (Table 2) are indicated by the horizontal spans.

According to the prediction for the transit ephemeris made by Bergmann et al. (2021), if HD 76920 b were to transit, it would have done so during TESS Sector 9. However, no clear transit signal was found by Bergmann et al. (2021) or in our data. Thus, we could not measure the planetary orbit or eccentricity through the TESS photometric data.

However, we can combine our newly computed asteroseismic stellar mass ($M_{\star,\rm seis} = 1.22 \pm 0.11 M_\odot$) with the orbital period, RV semi-amplitude and eccentricity values found by Bergmann et al. (2021) to compute updated values for the planet's semi-major axis and minimum mass. Using values from Bergmann et al. (2021), we find $a = 1.165 \pm 0.035$ au and $M_{\rm p} \sin i = 3.57 \pm 0.22\, M_{\rm Jup}$. These updated parameters place the orbital pericenter of the planet at 0.142 ± 0.005 au, revealing that the planet's orbit is sufficiently far from the star such that tidal decay is negligible until the star expands and engulfs the planet, in line with the findings of Bergmann et al. (2021).

The time at which the star will engulf the planet will depend on when the star begins ascending the RGB. During this phase of stellar evolution, the star's radius will expand to a distance approximately one order of magnitude greater than the planet's orbital pericenter, allowing the star to easily and quickly engulf the planet. The radius of our best-fitting model (Figure 6) will reach the planet's orbital pericenter in about 130 Myr.

We can also estimate the time at which the star starts ascending the RGB by using the `SSE` prescription from Hurley et al. (2000). According to this prescription, a $1.22\, M_\odot$ star with a metallicity of $Z = 0.02$ will begin the red giant phase at about 5.58 Gyr and leave it at 6.01 Gyr. During this interval, the planet will be engulfed. Asteroseismology has allowed us to estimate the current age of the star to be 5.2 ± 1.4 Gyr. This value clearly demonstrates that the star is on the verge of engulfing the planet. However, the uncertainty on the age is about triple the value of the duration of the red giant phase. Nevertheless, asteroseismology has also allowed us to constrain the stellar radius, and to a value of $8.68 \pm 0.34\, R_\odot$. This value corresponds to an age from the `SSE` model of 5.939 ± 0.004 Gyr, meaning that the planet will be engulfed in less than about 150 Myr. However, this approximate upper bound is likely an overestimate given the fact that the star's metallicity is sub-Solar.

Other stellar models produce similar results, just renormalized to other absolute ages within the measured asteroseismic uncertainty. For example, a $1.22\, M_\odot$ star with a sub-Solar metallicity of $Z = 0.01$ will begin the red giant phase at about 4.72 Gyr and leave it at 5.08 Gyr. In this case, the asteroseismically measured radius corresponds to an age from the `SSE` model of 5.007 ± 0.004 Gyr. This value illustrates that the planet will be engulfed within about 70 Myr. This result is in agreement with that of Bergmann et al. (2021).

6. CONCLUSIONS

In this work, we have analyzed the TESS photometric data for HD 76920 to determine the fundamental stellar parameters using asteroseismology, and to characterize the exoplanet system consisting of a planet with an extremely large orbital eccentricity. In total 5 sectors of TESS light curves are used for the extraction of asteroseismic parameters for the host star, including 12 individual oscillation frequencies. Modeling by various pipelines that utilize the extracted asteroseismic parameters, classical spectroscopic observables as well as luminosity from Gaia DR3 parallax, places strong constraints on the stellar parameters. Through the asteroseismic analysis, we obtain a value for the stellar mass of $1.22 \pm 0.11 M_\odot$, a stellar radius of $8.68 \pm 0.34\, R_\odot$ and an age of 5.2 ± 1.4 Gyr, which provide the most precise estimations for HD 76920 to date. The stellar models reveal that the star is ascending the red giant branch and most likely approaching closely to the luminosity bump where the properties of mixed-modes are significantly impacted by the buoyancy glitch. However, current power spectrum of HD 76920 from TESS does not allow for extraction of sufficient number of mixed modes that lead to the investigation of the buoyancy glitch.

The updated stellar parameters of the host star from our asteroseismic analysis have enabled improved estimations for the semi-major axis and mass of the planet as $a = 1.165 \pm 0.035$ au and $M_{\rm p} \sin i = 3.57 \pm 0.22\, M_{\rm Jup}$. With an orbital pericenter of 0.142 ± 0.005 au, we confirm that the planet is currently far away enough from the star to experience negligible tidal decay before being engulfed in the stellar envelope. However, we predict that this event will occur within about 100 Myr, depending on the stellar model used.

HD 76920 will be observed in 5 more sectors by TESS in Cycle 5. The prolonged data will possibly enable the detection of mixed-modes, and thus, the investigation of stellar interior through these modes. Moreover, our asteroseismic analysis emphasizes the potential of TESS for characterizing exoplanet systems through the synergy between exoplanet research and asteroseismology.

ACKNOWLEDGMENTS

The project leading to this publication has received funding from the B-type Strategic Priority Program of the Chinese Academy of Sciences (Grant No. XDB41000000). ADF acknowledges the support from the National Science Foundation Graduate Research Fellowship Program under Grant No. (DGE-1746045). M.S.L would like to acknowledge the support from VILLUM FONDEN (research grant 42101) and The Independent Research Fund Denmark's Inge Lehmann program (grant agreement no.: 1131-00014B). CK is supported by Erciyes University Scientific Research Projects Coordination Unit under grant number DOSAP MAP-2020-9749. T. Wu thanks the supports from the National Key Research and Development Program of China (Grant No. 2021YFA1600402), from the National Natural Science Foundation of China (Grant Nos. 11873084, 12133011, and 12273104), from Youth Innovation Promotion Association of Chinese Academy of Sciences, and from Ten Thousand Talents Program of Yunnan for Top-notch Young Talents. X.-Y. Zhang thanks the support from the National Natural Science Foundation of China (Grant No. 12173105). S.M. acknowledges support from the Spanish Ministry of Science and Innovation (MICINN) with the Ramón y Cajal fellowship no. RYC-2015-17697, grant no. PID2019-107187GB-I00 and PID2019-107061GB-C66, and through AEI under the Severo Ochoa Centres of Excellence Program 2020–2023 (CEX2019-000920-S). R.A.G. acknowledges the support from PLATO and GOLF CNES grants. This work was also supported by Fundação para a Ciência e a Tecnologia (FCT) through research grants UIDB/04434/2020 and UIDP/04434/2020. TLC is supported by FCT in the form of a work contract (CEECIND/00476/2018).

Facilities: TESS, Gaia

Software: `eleanor` (Feinstein et al. 2019), `lightkurve` (Lightkurve Collaboration et al. 2018), `TessCut` (Brasseur et al. 2019) , `LAURA` (De Moura et al. 2020), `FAMED` (Corsaro et al. 2020), `echelle`, `SolarlikePeakbagging` (Li et al. 2020), `apollinaire` (Breton et al. 2022), `fnpeaks`, `SYD` (Huber et al. 2009), `A2Z` (Mathur et al. 2010), `Period04` (Lenz & Breger 2005), `Yabox` (Mier 2017), `SEDEX` (Yu et al. 2021, 2022)

REFERENCES

Anders, F., Chiappini, C., Minchev, I., et al. 2017, A&A, 600, A70, doi: 10.1051/0004-6361/201629363

Angulo, C., Arnould, M., Rayet, M., et al. 1999, NuPhA, 656, 3, doi: 10.1016/S0375-9474(99)00030-5

Appourchaux, T., Chaplin, W. J., García, R. A., et al. 2012, A&A, 543, A54, doi: 10.1051/0004-6361/201218948

Asplund, M., Grevesse, N., Sauval, A. J., & Scott, P. 2009, ARA&A, 47, 481, doi: 10.1146/annurev.astro.46.060407.145222

Baglin, A., Auvergne, M., Boisnard, L., et al. 2006, in 36th COSPAR Scientific Assembly, Vol. 36, 3749

Ball, W. H., Chaplin, W. J., Schofield, M., et al. 2018, ApJS, 239, 34, doi: 10.3847/1538-4365/aaedbc

Ball, W. H., & Gizon, L. 2014, A&A, 568, A123, doi: 10.1051/0004-6361/201424325

Ballard, S., Chaplin, W. J., Charbonneau, D., et al. 2014, ApJ, 790, 12, doi: 10.1088/0004-637X/790/1/12

Beck, P. G., Montalban, J., Kallinger, T., et al. 2012, Nature, 481, 55, doi: 10.1038/nature10612

Bedding, T. R., Kjeldsen, H., Arentoft, T., et al. 2007, ApJ, 663, 1315, doi: 10.1086/518593

Bedding, T. R., Mosser, B., Huber, D., et al. 2011, Nature, 471, 608, doi: 10.1038/nature09935

Benomar, O., Masuda, K., Shibahashi, H., & Suto, Y. 2014, PASJ, 66, 94, doi: 10.1093/pasj/psu069

Bergmann, C., Jones, M. I., Zhao, J., et al. 2021, PASA, 38, E019, doi: 10.1017/pasa.2021.8

Borucki, W. J., Koch, D., Basri, G., et al. 2010, Science, 327, 977, doi: 10.1126/science.1185402

Brasseur, C. E., Phillip, C., Fleming, S. W., Mullally, S. E., & White, R. L. 2019, Astrocut: Tools for creating cutouts of TESS images. http://ascl.net/1905.007

Breton, S. N., García, R. A., Ballot, J., Delsanti, V., & Salabert, D. 2022, A&A, 663, A118, doi: 10.1051/0004-6361/202243330

Brown, T. M., & Gilliland, R. L. 1990, ApJ, 350, 839, doi: 10.1086/168435

Campante, T. L., Barros, S. C. C., Demangeon, O., et al. 2018, in PHysics of Oscillating STars. Proceedings from the PHOST (PHysics of Oscillating STars) symposium hosted by the Oceanographic Observatory in Banyuls-sur-mer (France) from 2-7 September 2018. This conference honours the life work of Professor Hiromoto Shibahashi, 50, doi: 10.5281/zenodo.2463210

Campante, T. L., Barclay, T., Swift, J. J., et al. 2015, ApJ, 799, 170, doi: 10.1088/0004-637X/799/2/170

Campante, T. L., Lund, M. N., Kuszlewicz, J. S., et al. 2016a, ApJ, 819, 85, doi: 10.3847/0004-637X/819/1/85
Campante, T. L., Schofield, M., Kuszlewicz, J. S., et al. 2016b, ApJ, 830, 138, doi: 10.3847/0004-637X/830/2/138
Campante, T. L., Veras, D., North, T. S. H., et al. 2017, MNRAS, 469, 1360, doi: 10.1093/mnras/stx876
Campante, T. L., Corsaro, E., Lund, M. N., et al. 2019, ApJ, 885, 31, doi: 10.3847/1538-4357/ab44a8
Casagrande, L., Silva Aguirre, V., Stello, D., et al. 2014, ApJ, 787, 110, doi: 10.1088/0004-637X/787/2/110
Casagrande, L., Silva Aguirre, V., Schlesinger, K. J., et al. 2016, MNRAS, 455, 987, doi: 10.1093/mnras/stv2320
Chaplin, W. J., Basu, S., Huber, D., et al. 2014, ApJS, 210, 1, doi: 10.1088/0067-0049/210/1/1
Christensen-Dalsgaard, J. 2008a, Ap&SS, 316, 13, doi: 10.1007/s10509-007-9675-5
—. 2008b, Ap&SS, 316, 113, doi: 10.1007/s10509-007-9689-z
Corsaro, E., & De Ridder, J. 2014, A&A, 571, A71, doi: 10.1051/0004-6361/201424181
Corsaro, E., De Ridder, J., & García, R. A. 2015, A&A, 579, A83, doi: 10.1051/0004-6361/201525895
Corsaro, E., McKeever, J. M., & Kuszlewicz, J. S. 2020, A&A, 640, A130, doi: 10.1051/0004-6361/202037930
Corsaro, E., Mathur, S., García, R. A., et al. 2017, A&A, 605, A3, doi: 10.1051/0004-6361/201731094
Cunha, M. S., Avelino, P. P., Christensen-Dalsgaard, J., et al. 2019, MNRAS, 490, 909, doi: 10.1093/mnras/stz2582
Cunha, M. S., Stello, D., Avelino, P. P., Christensen-Dalsgaard, J., & Townsend, R. H. D. 2015, ApJ, 805, 127, doi: 10.1088/0004-637X/805/2/127
Davies, G. R., & Miglio, A. 2016, Astronomische Nachrichten, 337, 774, doi: 10.1002/asna.201612371
De Moura, B. L., Beck, P. G., Di Mauro, M. P., et al. 2020, ApJ, 894, 67, doi: 10.3847/1538-4357/ab80c8
Feinstein, A. D., Montet, B. T., Foreman-Mackey, D., et al. 2019, PASP, 131, 094502, doi: 10.1088/1538-3873/ab291c
Ferguson, J. W., Alexander, D. R., Allard, F., et al. 2005, ApJ, 623, 585, doi: 10.1086/428642
Gaia Collaboration, Brown, A. G. A., Vallenari, A., et al. 2021, A&A, 649, A1, doi: 10.1051/0004-6361/202039657
Gilliland, R. L., McCullough, P. R., Nelan, E. P., et al. 2011, ApJ, 726, 2, doi: 10.1088/0004-637X/726/1/2
Grevesse, N., & Sauval, A. J. 1998, SSRv, 85, 161, doi: 10.1023/A:1005161325181
Gustafsson, B., Edvardsson, B., Eriksson, K., et al. 2008, A&A, 486, 951, doi: 10.1051/0004-6361:200809724
Handberg, R., Brogaard, K., Miglio, A., et al. 2017, MNRAS, 472, 979, doi: 10.1093/mnras/stx1929
Handberg, R., & Campante, T. L. 2011, A&A, 527, A56, doi: 10.1051/0004-6361/201015451
Harvey, J. 1985, in ESA Special Publication, Vol. 235, Future Missions in Solar, Heliospheric & Space Plasma Physics, ed. E. Rolfe & B. Battrick, 199
Hatt, E., Nielsen, M. B., Chaplin, W. J., et al. 2022, arXiv e-prints, arXiv:2210.09109. https://arxiv.org/abs/2210.09109
Hekker, S., Broomhall, A. M., Chaplin, W. J., et al. 2010, MNRAS, 402, 2049, doi: 10.1111/j.1365-2966.2009.16030.x
Hill, M. L., Kane, S. R., Campante, T. L., et al. 2021, AJ, 162, 211, doi: 10.3847/1538-3881/ac1b31
Houdek, G., Trampedach, R., Aarslev, M. J., & Christensen-Dalsgaard, J. 2017, MNRAS, 464, L124, doi: 10.1093/mnrasl/slw193
Houk, N., & Cowley, A. P. 1975, University of Michigan Catalogue of two-dimensional spectral types for the HD stars. Volume I. Declinations -90°.0 to -53°.0.
Huber, D. 2018, Synergies Between Asteroseismology and Exoplanetary Science, Astrophysics and Space Science Proceedings, 119–135, doi: 10.1007/978-3-319-59315-9_6
Huber, D., Stello, D., Bedding, T. R., et al. 2009, Communications in Asteroseismology, 160, 74. https://arxiv.org/abs/0910.2764
Huber, D., Carter, J. A., Barbieri, M., et al. 2013, Science, 342, 331, doi: 10.1126/science.1242066
Huber, D., Chaplin, W. J., Chontos, A., et al. 2019, AJ, 157, 245, doi: 10.3847/1538-3881/ab1488
Huber, D., White, T. R., Metcalfe, T. S., et al. 2022, AJ, 163, 79, doi: 10.3847/1538-3881/ac3000
Hurley, J. R., Pols, O. R., & Tout, C. A. 2000, MNRAS, 315, 543, doi: 10.1046/j.1365-8711.2000.03426.x
Iglesias, C. A., & Rogers, F. J. 1993, ApJ, 412, 752, doi: 10.1086/172958
—. 1996, ApJ, 464, 943, doi: 10.1086/177381
Jenkins, J. M., Twicken, J. D., McCauliff, S., et al. 2016, in Society of Photo-Optical Instrumentation Engineers (SPIE) Conference Series, Vol. 9913, Software and Cyberinfrastructure for Astronomy IV, ed. G. Chiozzi & J. C. Guzman, 99133E, doi: 10.1117/12.2233418
Jiang, C. 2015, PhD thesis, Stellar Astrophysics Centre, Aarhus University, Denmark
Jiang, C., Cunha, M., Christensen-Dalsgaard, J., & Zhang, Q. 2020a, MNRAS, 495, 621, doi: 10.1093/mnras/staa1285
Jiang, C., Cunha, M., Christensen-Dalsgaard, J., Zhang, Q. S., & Gizon, L. 2022, MNRAS, 515, 3853, doi: 10.1093/mnras/stac2065

Jiang, C., & Gizon, L. 2021, Research in Astronomy and Astrophysics, 21, 226, doi: 10.1088/1674-4527/21/9/226

Jiang, C., Jiang, B. W., Christensen-Dalsgaard, J., et al. 2011, ApJ, 742, 120, doi: 10.1088/0004-637X/742/2/120

Jiang, C., Bedding, T. R., Stassun, K. G., et al. 2020b, ApJ, 896, 65, doi: 10.3847/1538-4357/ab8f29

Kallinger, T., Beck, P. G., Stello, D., & Garcia, R. A. 2018, A&A, 616, A104, doi: 10.1051/0004-6361/201832831

Kallinger, T., Weiss, W. W., Barban, C., et al. 2010, A&A, 509, A77, doi: 10.1051/0004-6361/200811437

Kallinger, T., De Ridder, J., Hekker, S., et al. 2014, A&A, 570, A41, doi: 10.1051/0004-6361/201424313

Kamiaka, S., Benomar, O., Suto, Y., et al. 2019, AJ, 157, 137, doi: 10.3847/1538-3881/ab04a9

Kane, S. R., Ciardi, D. R., Gelino, D. M., & von Braun, K. 2012, MNRAS, 425, 757, doi: 10.1111/j.1365-2966.2012.21627.x

Kane, S. R., Bean, J. L., Campante, T. L., et al. 2021, PASP, 133, 014402, doi: 10.1088/1538-3873/abc610

Karoff, C. 2008, PhD thesis, Aarhus University

Kayhan, C., Yıldız, M., & Çelik Orhan, Z. 2019, MNRAS, 490, 1509, doi: 10.1093/mnras/stz2634

Kjeldsen, H., & Bedding, T. R. 1995, A&A, 293, 87. https://arxiv.org/abs/astro-ph/9403015

Kjeldsen, H., Bedding, T. R., & Christensen-Dalsgaard, J. 2008, ApJL, 683, L175, doi: 10.1086/591667

Kjeldsen, H., Bedding, T. R., Butler, R. P., et al. 2005, ApJ, 635, 1281, doi: 10.1086/497530

Kurucz, R. L. 1991, in NATO Advanced Study Institute (ASI) Series C, Vol. 341, Stellar Atmospheres - Beyond Classical Models, ed. L. Crivellari, I. Hubeny, & D. G. Hummer, 441

Lenz, P., & Breger, M. 2005, Communications in Asteroseismology, 146, 53, doi: 10.1553/cia146s53

Li, Y., Bedding, T. R., Li, T., et al. 2020, MNRAS, 495, 2363, doi: 10.1093/mnras/staa1335

Lightkurve Collaboration, Cardoso, J. V. d. M., Hedges, C., et al. 2018, Lightkurve: Kepler and TESS time series analysis in Python. http://ascl.net/1812.013

Lund, M. N., Lundkvist, M., Silva Aguirre, V., et al. 2014, A&A, 570, A54, doi: 10.1051/0004-6361/201424326

Lund, M. N., Silva Aguirre, V., Davies, G. R., et al. 2017, ApJ, 835, 172, doi: 10.3847/1538-4357/835/2/172

Lundkvist, M. S. 2015, PhD thesis, Stellar Astrophysics Centre, Aarhus University, Denmark

Lundkvist, M. S., Kjeldsen, H., Albrecht, S., et al. 2016, Nature Communications, 7, 11201, doi: 10.1038/ncomms11201

Mathur, S., García, R. A., Régulo, C., et al. 2010, A&A, 511, A46, doi: 10.1051/0004-6361/200913266

Mathur, S., Metcalfe, T. S., Woitaszek, M., et al. 2012, ApJ, 749, 152, doi: 10.1088/0004-637X/749/2/152

Metcalfe, T. S., Monteiro, M. J. P. F. G., Thompson, M. J., et al. 2010, ApJ, 723, 1583, doi: 10.1088/0004-637X/723/2/1583

Mier, P. R. 2017, Pablormier/Yabox: V1.0.3, v1.0.3, Zenodo, Zenodo, doi: 10.5281/zenodo.848679

Mosser, B., & Appourchaux, T. 2009, A&A, 508, 877, doi: 10.1051/0004-6361/200912944

Mosser, B., Goupil, M. J., Belkacem, K., et al. 2012, A&A, 540, A143, doi: 10.1051/0004-6361/201118519

Nielsen, M. B., Ball, W. H., Standing, M. R., et al. 2020, A&A, 641, A25, doi: 10.1051/0004-6361/202037461

Paxton, B., Bildsten, L., Dotter, A., et al. 2011, ApJS, 192, 3, doi: 10.1088/0067-0049/192/1/3

Paxton, B., Cantiello, M., Arras, P., et al. 2013, ApJS, 208, 4, doi: 10.1088/0067-0049/208/1/4

Paxton, B., Marchant, P., Schwab, J., et al. 2015, ApJS, 220, 15, doi: 10.1088/0067-0049/220/1/15

Pinçon, C., Goupil, M. J., & Belkacem, K. 2020, A&A, 634, A68, doi: 10.1051/0004-6361/201936864

Pinsonneault, M. H., Elsworth, Y., Epstein, C., et al. 2014, ApJS, 215, 19, doi: 10.1088/0067-0049/215/2/19

Pinsonneault, M. H., Elsworth, Y. P., Tayar, J., et al. 2018, ApJS, 239, 32, doi: 10.3847/1538-4365/aaebfd

Rendle, B. M., Buldgen, G., Miglio, A., et al. 2019, MNRAS, 484, 771, doi: 10.1093/mnras/stz031

Ricker, G. R., Winn, J. N., Vanderspek, R., et al. 2015, Journal of Astronomical Telescopes, Instruments, and Systems, 1, 014003, doi: 10.1117/1.Jatis.1.1.014003

Rodrigues, T. S., Girardi, L., Miglio, A., et al. 2014, MNRAS, 445, 2758, doi: 10.1093/mnras/stu1907

Rogers, F. J., & Nayfonov, A. 2002, ApJ, 576, 1064, doi: 10.1086/341894

Roxburgh, I. W. 2017, A&A, 604, A42, doi: 10.1051/0004-6361/201731057

Schlegel, D. J., Finkbeiner, D. P., & Davis, M. 1998, ApJ, 500, 525, doi: 10.1086/305772

Schofield, M., Chaplin, W. J., Huber, D., et al. 2019, ApJS, 241, 12, doi: 10.3847/1538-4365/ab04f5

Serenelli, A., Johnson, J., Huber, D., et al. 2017, ApJS, 233, 23, doi: 10.3847/1538-4365/aa97df

Sharma, S., Stello, D., Bland-Hawthorn, J., Huber, D., & Bedding, T. R. 2016, ApJ, 822, 15, doi: 10.3847/0004-637X/822/1/15

Silva Aguirre, V., Casagrande, L., Basu, S., et al. 2012, ApJ, 757, 99, doi: 10.1088/0004-637X/757/1/99

Silva Aguirre, V., Lund, M. N., Antia, H. M., et al. 2017, ApJ, 835, 173, doi: 10.3847/1538-4357/835/2/173

Sliski, D. H., & Kipping, D. M. 2014, ApJ, 788, 148, doi: 10.1088/0004-637X/788/2/148
Stassun, K. G., Collins, K. A., & Gaudi, B. S. 2017, AJ, 153, 136, doi: 10.3847/1538-3881/aa5df3
Stassun, K. G., Corsaro, E., Pepper, J. A., & Gaudi, B. S. 2018, AJ, 155, 22, doi: 10.3847/1538-3881/aa998a
Stassun, K. G., & Torres, G. 2016, AJ, 152, 180, doi: 10.3847/0004-6256/152/6/180
—. 2021, ApJL, 907, L33, doi: 10.3847/2041-8213/abdaad
Stassun, K. G., Oelkers, R. J., Pepper, J., et al. 2018b, AJ, 156, 102, doi: 10.3847/1538-3881/aad050
Stello, D., Bruntt, H., Preston, H., & Buzasi, D. 2008, ApJL, 674, L53, doi: 10.1086/528936
Thoul, A. A., Bahcall, J. N., & Loeb, A. 1994, ApJ, 421, 828, doi: 10.1086/173695
Torres, G., Andersen, J., & Giménez, A. 2010, A&A Rv, 18, 67, doi: 10.1007/s00159-009-0025-1
Townsend, R. H. D., & Teitler, S. A. 2013, MNRAS, 435, 3406, doi: 10.1093/mnras/stt1533
Van Eylen, V., & Albrecht, S. 2015, ApJ, 808, 126, doi: 10.1088/0004-637X/808/2/126
Van Eylen, V., Albrecht, S., Huang, X., et al. 2019, AJ, 157, 61, doi: 10.3847/1538-3881/aaf22f
van Leeuwen, F. 2007, A&A, 474, 653, doi: 10.1051/0004-6361:20078357
Viani, L. S., Basu, S., Corsaro, E., Ball, W. H., & Chaplin, W. J. 2019, ApJ, 879, 33, doi: 10.3847/1538-4357/ab232e
Vrard, M., Mosser, B., Barban, C., et al. 2015, A&A, 579, A84, doi: 10.1051/0004-6361/201425064
Wittenmyer, R. A., Jones, M. I., Horner, J., et al. 2017, AJ, 154, 274, doi: 10.3847/1538-3881/aa9894
Wu, T., & Li, Y. 2019, ApJ, 881, 86, doi: 10.3847/1538-4357/ab2ad8
Yıldız, M., Çelik Orhan, Z., & Kayhan, C. 2019, MNRAS, 489, 1753, doi: 10.1093/mnras/stz2223
Yu, J., Hekker, S., Bedding, T. R., et al. 2021, MNRAS, 501, 5135, doi: 10.1093/mnras/staa3970
Yu, J., Huber, D., Bedding, T. R., et al. 2018, ApJS, 236, 42, doi: 10.3847/1538-4365/aaaf74
Yu, J., Khanna, S., Themessl, N., et al. 2022, arXiv e-prints, arXiv:2206.00046. https://arxiv.org/abs/2206.00046
Zhang, X., Cai, T., Li, Y., & Wu, T. 2022, ApJ, 931, 64, doi: 10.3847/1538-4357/ac695b